PCCP

Accepted Manuscript

This is an *Accepted Manuscript*, which has been through the Royal Society of Chemistry peer review process and has been accepted for publication.

Accepted Manuscripts are published online shortly after acceptance, before technical editing, formatting and proof reading. Using this free service, authors can make their results available to the community, in citable form, before we publish the edited article. We will replace this *Accepted Manuscript* with the edited and formatted *Advance Article* as soon as it is available.

You can find more information about *Accepted Manuscripts* in the Information for Authors.

Please note that technical editing may introduce minor changes to the text and/or graphics, which may alter content. The journal's standard Terms & Conditions and the Ethical guidelines still apply. In no event shall the Royal Society of Chemistry be held responsible for any errors or omissions in this *Accepted Manuscript* or any consequences arising from the use of any information it contains.

ROYAL SOCIETY OF CHEMISTRY

www.rsc.org/pccp

PCCP RSCPublishing

COMMUNICATION

Cite this: DOI: 10.1039/x0xx00000x

An Asymmetric Naphthalimide Derivative for n-Channel Organic Field-Effect Transistors

Zongrui Wang,[ab] Jianfeng Zhao,[cd] Huanli Dong,*[ae] Ge Qiu,[ae] Qichun Zhang,*[cf] and Wenping Hu*[a]

Received 00th January 2012,
Accepted 00th January 2012

DOI: 10.1039/x0xx00000x

www.rsc.org/

A new naphthalene diimides (NDI) derivative with asymmetric aromatic backbone 2-tetradecylbenzo[*lmn*] benzo[4,5]imidazo[2,1-*b*][3,8]phenanthroline-1,3,6(2*H*)-trione (IZ0) is designed and synthesized. Low LUMO level, large energy gap and high thermal stability are characterized for IZ0 compound. The OFET devices based on IZ0 semiconductor exhibit typical n-type behavior. Through continuously optimizing the fabrication conditions, high performance n-channel OFETs are fabricated based on IZ0 films and single crystals, with the highest carrier mobility of 0.072 cm^2 V^{-1} s^{-1} and 0.22 cm^2 V^{-1} s^{-1}, respectively.

Organic field effect transistors (OFETs), due to their great potential applications in the low-cost, flexible and large-area electronics, have attracted extensive academic and commercial interest in the past decades.[1-4] To date, great advances have been achieved for p-type OFETs, and their mobilities are comparable to or even surpassing that of amorphous silicon thanks to the significant development of p-type semiconducting materials to a great extent.[1,5-9] While in comparison, the number of electron transporting n-type materials and their device performance are relatively lagged behind.[1,10-13] Thus, searching for new n-type organic semiconductors to construct high performance n-channel devices is still very imperative for the development of complementary circuits in organic electronics.

Naphthalene diimides (NDI) are regarded as one of the promising unit cores for n-channel semiconducting materials due to their large electron affinities, ideal planar conjugated structure as well as the easy tunability of photoelectrical properties with substituents at the imide N atoms or p-system cores.[11-19] Various NDI-based electron-transporting semiconductors with symmetric molecular structure have been successfully designed and synthesized.[11-14] Design of asymmetric conjugated organic molecules has recently been found to be an another promising strategy for high efficient hole-transporting materials due to their better self-organization ability for formation of large-size crystalline domains.[20-23] Given this, for n-channel materials, asymmetric NDI-core based derivatives also gradually attract people's attention in recent years.[24-37] For example, Oritz *et al*[30] designed and synthesized a series of asymmetric arylenediimide-thiophene derivatives, and a high electron mobility of 0.35 cm^2 V^{-1} s^{-1} is obtained. Deng *et al*[25] synthesized 1,8-naphthoylene(trifluoromethylbenzimidazole)-4,5-dicarboxylic acid imide derivatives, which demonstrate an electron mobility of 0.1 cm^2 V^{-1} s^{-1} for thin film transistors with Ca as the source/drain electrodes. Encouraged by the previous works in this field, here, a new asymmetric NDI-based organic semiconductor 2-tetradecylbenzo[*lmn*]benzo[4,5]imidazo[2,1-*b*][3,8]phenanthroline-1,3,6(2*H*)-trione (IZ0, Scheme 1) is synthesized and investigated for its application in field-effect transistors. The design of IZ0 compound is based on the following considerations: i) extending the conjugated planes and lowering the lowest unoccupied molecular orbital (LUMO) level with the introduction of an electron deficient moiety of fused aromatic benzimidazole on one side of NDI core,[38-42] ii) improving the solubility and molecular self-assembly properties with substituent of long alkyl chain on the other side of NDI-imide N atom.[21,43]

IZ0 is synthesized in a similar way to the reported literatures[35,44] with a slight modification. Scheme 1 shows the synthesis route of IZ0 compound. After the condensation reaction between compound **2** and benzene-1,2-diamine **3**, IZ0 solid is obtained and characterized

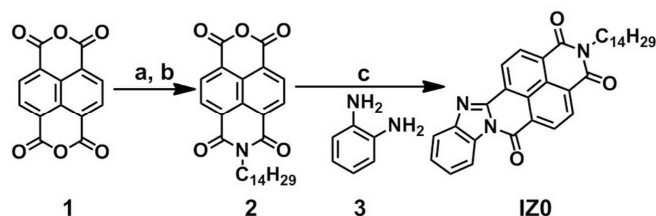

Scheme 1 The synthesis of 2-tetradecylbenzo[*lmn*]benzo[4,5]imidazo[2,1-*b*][3,8]phenanthroline-1,3,6(2*H*)-trione (IZ0). Conditions: a) Tetradecane-1-amine, *iso*-propanol/H_2O, 50 ?; b) HOAc, reflux, 4h; c) Pyridine, reflux, 4h, N_2.

Physical Chemistry Chemical Physics Accepted Manuscript

This journal is © The Royal Society of Chemistry 2012

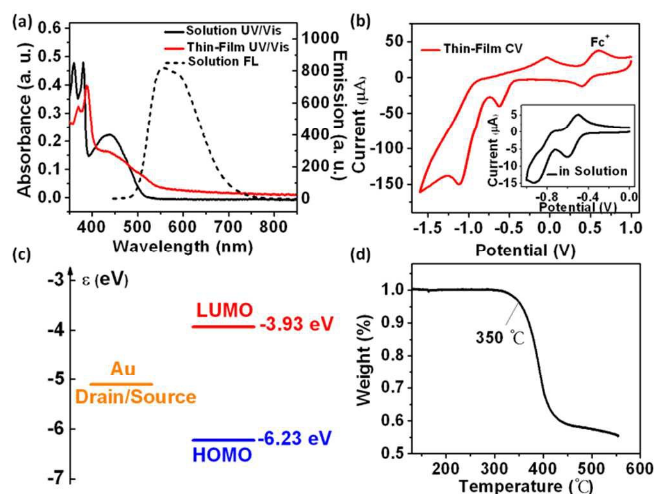

Fig. 1 (a) UV-*vis* spectra and fluorescence spectra of IZ0 in solution (black) and film (red). (b) Cyclic voltammogram of IZ0 in thin film (red) and solution (inset) . (c) The plot of energy level diagram of IZ0 and Au electrodes. (d) TGA curve of IZ0 compound with a heating rate of 10 ℃ min^{-1} under nitrogen.

by ^{1}H-NMR spectra, matrix-assisted laser desorption/ionization time-of-flight (MALDI-TOF), high-resolution mass spectrometry and infrared spectroscopy (IR) (see Supporting information Fig. S1-S4).

The UV-*vis* absorption spectra of IZ0 in CH_2Cl_2 solution is shown in Fig. 1a, which demonstrates a broad absorption peak at 437 nm, corresponding to the n-π* transition.[34] In comparison with IZ0 solution, UV-*vis* of vacuum-deposited IZ0 film shows a bathochromic shift from 510 nm to 539 nm (the onset of broad absorptions), indicating relatively good molecular organization in film.[34,36] With 427 nm exciting light, the fluorescence spectrum of IZ0 solution exhibits a strong emission in the range of 500 nm to 700 nm, which might originate from the synergic effect of the electron-deficient bisimide unit and the fused benzimidazole moiety.[26] A large energy gap (E_g^{opt}) of 2.30 eV for IZ0 is calculated from the lowest-energy absorption edge of the film, suggesting its good photostability. Fig. 1b shows the cyclic voltammetry (CV) of IZ0, which is performed in dry CH_2Cl_2 solution with ITO as the working electrode, Ag/AgCl as the reference electrode and vacuum-deposited IZ0 film on ITO. Estimated from the onset position of the reductive peak in CV, a relatively low LUMO level of -3.93 eV is calculated for IZ0. The HOMO level was obtained by $E_{HOMO} = E_{LUMO} - E_g^{opt}$. For comparison, the CV behavior of IZ0 in solution is shown in inset of Fig. 1b, which is well consistent with that of IZ0 films. In addition, density function theory (DFT) calculation is also carried out at the B3LYP/6-311 G** level using Gaussian 09 Software (as shown in Fig. S5) to help us well understand the electronic structure of IZ0. The results show that the LUMO level is mainly localized on the imide-substituted naphthalene part, while the HOMO is more inclined to spread over the whole molecule, probably due to the asymmetric effect of IZ0 molecular structure. Fig. 1c shows the comparison of energy levels of IZ0 and Au electrode. The thermal property of IZ0 is investigated by thermogravimetric analysis (TGA), as shown in Fig. 1d, which shows the high decomposition temperature of 350 °C, indicating its good thermal stability.

Table 1. OFET characteristics of IZ0 vacuum-deposited thin films (50 nm) at different substrate conditions.

Substrate	T_{sub} (°C)		μ (cm^2/Vs)	I_{on}/I_{off}	V_t(V)
Bare	25	μ_{ave}	8.38×10^{-5}	1.87×10^{4}	59.4
		μ_{max}	1.01×10^{-4}	2.18×10^{4}	58.5
	60	μ_{ave}	1.61×10^{-3}	5.18×10^{5}	45.0
		μ_{max}	1.94×10^{-3}	2.41×10^{5}	56.8
	90	μ_{ave}	5.10×10^{-4}	3.02×10^{6}	53.3
		μ_{max}	5.91×10^{-4}	3.46×10^{5}	55.6
HMDS	25	μ_{ave}	5.38×10^{-4}	1.00×10^{5}	23.2
		μ_{max}	8.71×10^{-4}	4.76×10^{4}	22.6
	60	μ_{ave}	2.30×10^{-3}	3.89×10^{6}	38.9
		μ_{max}	2.96×10^{-3}	4.39×10^{6}	35.3
	90	μ_{ave}	4.44×10^{-4}	9.93×10^{5}	48.5
		μ_{max}	5.81×10^{-4}	2.02×10^{6}	53.7
OTS	25	μ_{ave}	5.07×10^{-3}	6.12×10^{5}	42.2
		μ_{max}	1.05×10^{-2}	7.36×10^{5}	55.3
	60	μ_{ave}	2.83×10^{-3}	3.03×10^{6}	32.8
		μ_{max}	5.94×10^{-3}	1.78×10^{6}	53.9
	90	μ_{ave}	7.00×10^{-3}	1.45×10^{7}	47.8
		μ_{max}	1.12×10^{-2}	2.14×10^{7}	52.5
OTMS	25	μ_{ave}	9.96×10^{-3}	1.08×10^{6}	32.5
		μ_{max}	1.45×10^{-2}	3.03×10^{6}	40.9
	60	μ_{ave}	1.96×10^{-2}	3.94×10^{6}	31.4
		μ_{max}	2.01×10^{-2}	3.13×10^{6}	26.5
	90	μ_{ave}	2.87×10^{-2}	6.25×10^{7}	53.5
		μ_{max}	3.33×10^{-2}	9.94×10^{7}	52.9

Bottom-gate top-contact OFETs based on vacuum-deposited IZ0 films are fabricated to investigate its field-effect properties. It is well known that the surface property of substrate and vacuum-deposited temperature has significant influence on the OFET performance.[45-49] So here we systematically investigate the effect of different experimental conditions on the performance of IZ0-OFETs. The detailed device performances for IZ0 OFETs are summarized in Table 1. As expected that all the IZ0-OFET devices including that on bare-SiO_2 substrate exhibit typical n-channel transporting properties. Through modifying the SiO_2 substrate with self-assembly monolayers (SAMs), such as hexamethyldisilazane (HMDS), octadecyltrichlorosilane (OTS) and octadecyltrimethoxysilane (OTMS), the IZ0-OFET performances are significantly improved by 1-2 orders of magnitude probably due to the reduce of electron traps such as OH- on the bare substrate and the improvement of film morphologies on the hydrophobic nature of modified-substrate surface for better compatible semiconductor/dielectric interface, [46-50] which will be discussed in detail according to their AFM morphologies of IZ0 films. Moreover, the device performance can also be further increased by modulating the temperature (T_{sub}) of vacuum-deposited substrates due to the increase of film crystallinity. The detailed films morphology and crystallinity of IZ0 will be characterized and discussed in following. Through continuously optimizing the device fabrication conditions, a high charge carrier mobility of 0.033 cm^2 V^{-1} s^{-1} is achieved finally for vacuum-

Physical Chemistry Chemical Physics Accepted Manuscript

This journal is © The Royal Society of Chemistry 2012

deposited IZ0 films based on OTMS-modified SiO_2 substrate with deposition temperature of 90 °C. The representative transfer and output characteristics for IZ0-film transistor are demonstrated in Fig. S6. The relatively high V_T in these devices is due to the mismatched energy levels between the Au electrodes (-5.1 eV) and LUMO levels (-3.93 eV) of IZ0 (Fig. 1c).

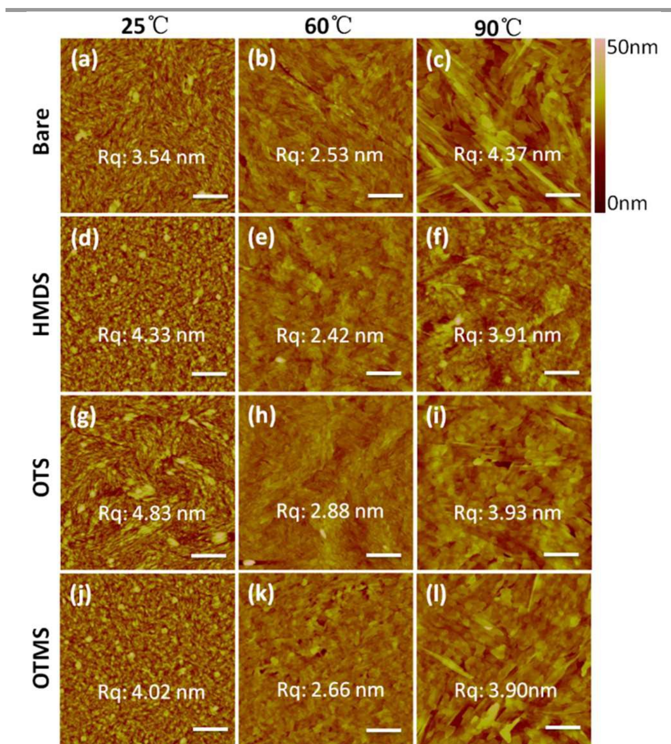

Fig. 2 AFM images of vacuum-deposited IZ0 thin films (50 nm) on different experiment conditions. (a, b, and c) on unmodified bare SiO_2 substrate, (d, e and f) on HMDS-modified substrate, (g, h, and i) on OTS-modified substrate, and (j, k and l) on OTMS-modified substrates at the deposition temperatures of 25 °C , 60 °C and 90 °C. Inst: Rq refers to the root-mean-square roughness, scale bar: 1 μm.

Atomic force microscope (AFM) and X-ray diffraction (XRD) are carried out to understand the effect of fabrication conditions on IZ0-film OFET performance. Fig. 2 shows the AFM morphology images of IZ0 films prepared in different conditions, including the SAM modification and the substrate temperature. In parallel comparison for films on different substrates but under the same deposition condition, there are not obvious morphology changes for IZ0 films based on bare SiO_2 to SAM-modified SiO_2 substrate, suggesting weak substrate effect of IZ0 film growth on substrates, which is also further confirmed by reducing the thickness of IZ0 films (Fig. S7). It can seen that well-defined terrace-type IZ0 films can be obtained on all the substrates in the first few layer at the interface. For example, on OTS- and OTMS-modified substrates, highly continuous IZ0 films are obtained, which are favorable for efficient charge transport to ensure high device performance (Fig. S8). While on HMDS-modified substrate, the IZ0 films becomes relatively discontinuous though still demonstrating the terrace-type growth mode, thus leading to inferior device performance compared to OTS- and OTMS-modified substrates (Table S1). For devices on bare SiO_2 substrate, although well-defined and continuous films are also obtained, the high-density OH-electron traps existing in the substrate results in the worst device performance (Table S1).[49] In comparison, IZ0 film growth demonstrates strong dependence on the substrate temperature. Obviously, at room temperature, small and granular grains form in IZ0 films, while with the increase of substrate temperature, the sizes of crystalline domains also increase. At 90°C deposition temperature, the crystalline domains exhibit terrace-like step structures with the sizes up to hundreds of nanometers, indicating the typical lamellar growth model. The increased grain size suggest the enhanced film crystallinity and reduced boundary density in films, which are beneficial for efficient charge transport and the achievement of good OFET performance.[18] However, on bare-SiO_2 and HMDS-modified substrates, an inverse device performance change is demonstrated at 90 °C compared with that at 60 °C, which is largely due to the increase of grain boundary resulting in discontinuous films. In comparison, good film continuity is still maintained though with the increase of crystalline domain size, thus leading to the better device performance at 90 °C deposition temperature.

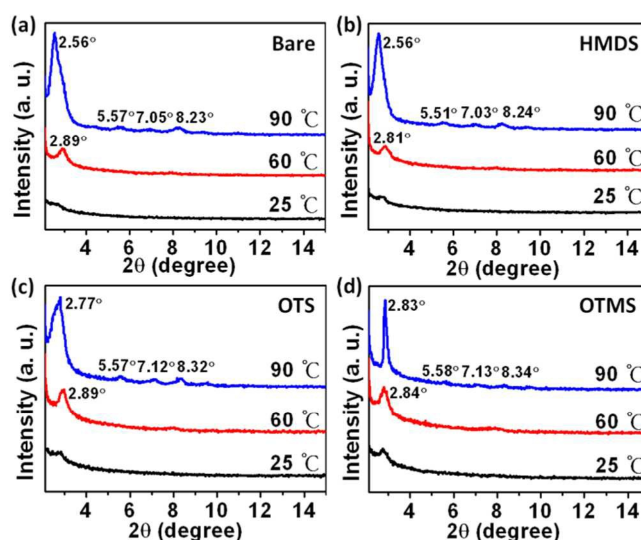

Fig. 3 X-ray diffraction patterns of IZ0 vacuum-deposited thin films (a) on unmodified bare SiO_2 substrate, (b) on HMDS-modified substrate , (c), on OTS-modified substrate and (d) on OTMS-modified substrates.

Besides the dependence of film morphology on substrate surface property, the film crystallinity is also strongly dependent on the substrate temperature. As shown in Fig. 3, with the increase of substrate temperature, the crystallinity of IZ0 films on all the substrates is obviously enhanced not only with the increase of intensity for the first diffraction peak at small 2-theta angle but also with the presence of new-ordered diffraction peaks in the large 2-theta angle region. The estimated *d*-spacing of ~ 3.1 nm from the first diffraction peak of 2θ ~ 2.9° for IZO films is larger than that of IZO-molecule length (2.60 nm, Fig. S9a) but much smaller than the twice of two-molecular length (5.2 nm), suggesting a bilayer packing of IZ0 molecules in films, where the asymmetric molecules are alternately in the opposite directions with alkyl-chain interdigitation (Fig. S9b), as manifested by other reported asymmetric organic semiconductors.[21,22] Moreover, in this molecular packing model, the π-π stacking direction is just parallel to the substrate (Fig. S9b), which is beneficial for charge transport. Additionally, one interesting phenomenon observed is that for 90 °C substrate temperature, the

Physical Chemistry Chemical Physics Accepted Manuscript

layer *d*-spacing is obviously increased for IZ0 films on bare-SiO_2 and HMDS-modified substrate with the diffraction 2-theta angle from 2.89° to 2.56°. This result suggests that there is a large molecular packing changes for IZ0 films on bare-SiO_2 and HMDS-modified substrates with the increase of substrate temperature, possibly with more-stretched alkyl chains, which is in some extent unfavorable for vertical charge transport (injection and extraction) between neighboring layers because of the large effect of bulky insulating layers.[51] While on OTS- and OTMS-modified substrate, in contrast, there is a slight change for the interlayer distance except for the increase of crystallinity. This structure changes of molecular packing for IZ0 films on different substrates from 60 °C to 90 °C deposition temperature is also clearly reflected by their previous AFM film morphology changes shown in Fig. 2, with the presence of relatively large grain boundary for films on bare-SiO_2 and HMDS-modified substrates at 90 °C while the good maintaince of film continuity for films on OTS- and OTMS-modified substrates. All the characterizations demonstrate that the obtained good device performance of IZ0-film OFETs on OTS- and OTMS-modified substrates is due to the combining effects of low-density electron traps on interface, the continuous films with relatively large domain size as well as the high crystallinity of IZ0-films.

Moreover, large-size high quality crystalline IZ0 films with significantly reduced grain boundaries are further obtained on OTS-modified substrate in our experiment by controlling the deposition process through physical vapor transport (PVT) technique,[52] as shown in Fig. 4a and 4b. The d-spacing of 3.1 ± 0.2 nm estimated from AFM results is well consistent with that of ~3.3 nm obtained from the first-order diffraction of 2.70° in XRD pattern (Fig. 4b). Such two-dimensional polycrystalline thin film with very smooth surface roughness (~0.30 nm), and more regular molecular packing characterized by its XRD patterns (Fig. S10) indicates the more beneficial for charge transport and high device performance. In order to largely reduce the grain boundaries in conducting channel, here we try to decrease the channel length to 25 μm with a corresponding width of 200 μm for IZ0-OFET device fabrication. As expected that the device performance is further increased by 6 times magnitude and the mobility for IZ0-film OFETs is up to 0.072 $cm^2\ V^{-1}\ s^{-1}$, which is due to the reduced grain boundaries in transistor conducting channel and more ordered molecular packing in such films.

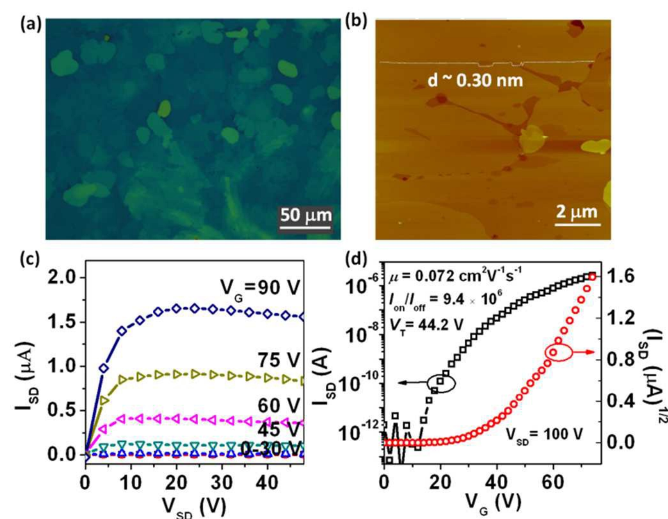

Fig. 4 (a) Optical microscopy image and (b) AFM topography imager of two-dimensional IZ0 crystalline films prepared from PVT method. Scale bar in a: 50 μm. (c) Typical output and (d) transfer characteristics of OFETs based on the IZ0 crystalline films.

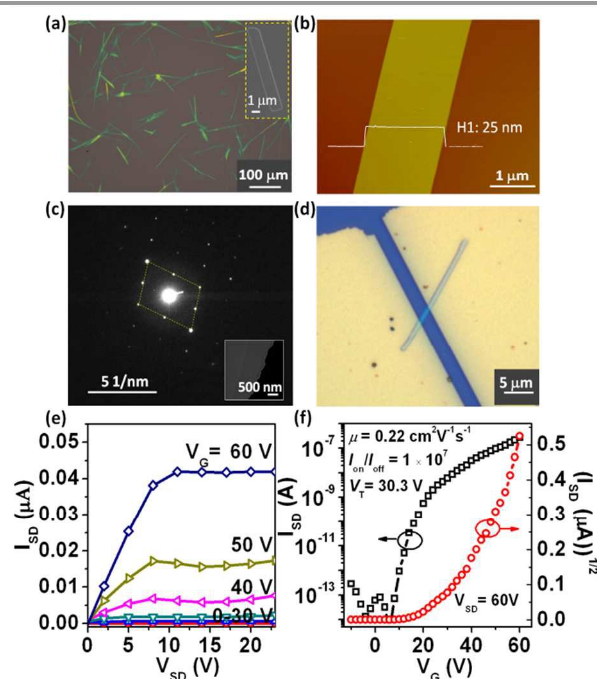

Fig. 5 (a) Optical micrograph of IZ0 single crystalline micro-ribbons grown from PVT and inset is the SEM image of an individual IZ0 single micro-ribbon. (b) AFM image of a single micro-ribbon and inset is the corresponding height cross-section. (c) TEM image (inset) and the corresponding SAED patterns of IZ0 micro-ribbon. (d) Microscopy image of a real IZ0 single crystal organic field effect transistor fabricated from "organic ribbon mask technique". (e,f) Representative output and transfer characteristics of IZ0 single crystal transistors.

It is well known that single crystals are the best candidates for investigation of the intrinsic charge transport properties of materials and fabrication of high performance devices due to no grain boundary, no defects and long-range molecular orders.[53,54] Based on this consideration, here large-area, high quality single crystals of IZ0 are further produced through PVT process. Fig. 5a shows the optical and scanning electron microscope (SEM) images of the obtained IZ0 crystals, which demonstrate regular ribbon shape with the length of tens to hundred micrometers. As characterized by AFM (Fig. 5b), the IZ0 crystal exhibits well-defined cross section, a low root-mean-square of 0.3-0.5 nm and a thin thickness of around 25 nm. Fig. 5c and 5d show the TEM of an individual IZ0 crystal and its corresponding selected area electron diffraction (SAED) pattern, confirming the typical single crystal characteristic of IZ0 crystal. It's a pity that because we don't have the single crystal data of IZ0, it is difficult for us to index these diffraction spots. Nevertheless, the high quality and single crystal property of IZ0 crystals suggest its high charge carrier transport in devices. Through an "organic ribbon mask technique",[55] top-contact bottom-gate IZ0 single crystal OFETs are constructed. Fig. 5d shows the optical microscopy of a representative IZ0 crystal transistor, with the channel length and width of 2.70 μm and 0.90 μm, respectively. Fig. 5e and 5f demonstrate the typical output and transfer characteristics of IZ0

Physical Chemistry Chemical Physics Accepted Manuscript

 This journal is © The Royal Society of Chemistry 2012

single crystal transistors. The highest field-effect mobility for IZ0 single crystal transistors is 0.22 cm^2 V^{-1} s^{-1}, which is about 3 times higher than that of two-dimensional crystalline films and one order of magnitude than that of traditionally-deposited films. Furthermore, it is found that the crystal micro-ribbons of IZ0 also exhibit bright fluorescence characteristic under the illumination of ultraviolet light (Fig. S11), indicating its potential application in the optoelectronic devices, and corresponding studies are still underway.

Conclusions

In conclusion, a novel asymmetric naphthalimide derivative is designed and synthesized. Through continuously optimizing the fabrication conditions, high performance n-channel OFETs are fabricated based on IZ0 films and single crystals, with the highest carrier mobility of 0.072 cm^2 V^{-1} s^{-1} and 0.22 cm^2 V^{-1} s^{-1}, respectively, which is one of the highest values reported for asymmetric n-type organic semiconductors.

Acknowledgements

The authors acknowledge National Natural Science Foundation of China (51222306, 91222203, 91233205, 91433115), the China-Denmark Co-project (60911130231), TRR61 (NSFC-DFG Transregio Project), the Ministry of Science and Technology of China (2011CB808405, 2013CB933403, 2013CB933504), the Strategic Priority Research Program of the Chinese Academy of Sciences (XDB12030300), Beijing NOVA Programme (Z131101000413038), Beijing Local College Innovation Team Improve Plan (IDHT20140512), and Chinese Academy of Sciences. J. Z. acknowledges financial support from Jiangsu Province Science Foundation for Youths (BK20130912) Q.Z. acknowledges financial support from AcRF Tier 1 (RG 16/12) and Tier 2 (ARC 20/12 and ARC 2/13) from MOE, and the CREATE program (Nanomaterials for Energy and Water Management) from NRF, Singapore.

Notes and references

[a] Beijing National Laboratory for Molecular Sciences, Key Laboratory of Organic Solids, Institute of Chemistry, Chinese Academy of Sciences, Beijing 100190, P. R. China

Email: dhl522@iccas.ac.cn, huwp@iccas.ac.cn

[b] University of Chinese Academy of Sciences, Beijing 100049, P. R. China

[c] School of Materials Science & Engineering, Nanyang Technological University, 50 Nanyang Avenue, Singapore 639798, Singapore

Email: qczhang@ntu.edu.sg

[d] Key Laboratory of Flexible Electronics & Institute of Advanced Materials, Jiangsu National Synergistic Innovation Center for Advanced Materials, Nanjing Tech University, 30 South Puzhu Road, Nanjing 211816, P.R. China

[e] Department of Chemistry, Capital Normal University, Beijing 100048, P. R. China

[f] Division of Chemistry and Biological Chemistry, School of Physical and Mathematical Sciences, Nanyang Technological University, Singapore 63731, Singapore

Electronic Supplementary Information (ESI) available. See DOI: 10.1039/c000000x/

1 C. Wang, H. Dong, W. Hu, Y. Liu and D. Zhu, *Chem. Rev.*, 2012, **112**, 2208.
2 H. Yan, Z. Chen, Y. Zheng, C. Newman, J. R. Quinn, F. Dotz, M. Kastler and A. Facchetti, *Nature*, 2009, **457**, 679.
3 B. Crone, A. Dodabalapur, Y. Y. Lin, R. W. Filas, Z. Bao, A. LaDuca, R. Sarpeshkar, H. E. Katz and W. Li, *Nature*, 2000, **403**, 521.
4 M. Muccini, *Nat. Mater.*, 2006, **5**, 605.
5 H. Dong, X. Fu, J. Liu, Z. Wang and W. Hu, *Adv. Mater.*, 2013, **25**, 6158.
6 Y. Yuan, G. Giri, A. L. Ayzner, A. P. Zoombelt, S. C. B. Mannsfeld, J. Chen, D. Nordlund, M. F. Toney, J. Huang and Z. Bao, *Nat Commun*, 2014, **5**, 3005.
7 L. Zhang, A. Fonari, Y. Liu, A.-L. M. Hoyt, H. Lee, D. Granger, S. Parkin, T. P. Russell, J. E. Anthony, J.-L. Brédas, V. Coropceanu and A. L. Briseno, *J. Am. Chem. Soc.*, 2014, **136**, 9248.
8 G. Kim, S. J. Kang, G. K. Dutta, Y.-K. Han, T. J. Shin, Y.-Y. Noh and C. Yang, *J. Am. Chem. Soc.*, 2014, **136**, 9477.
9 P. He, Z. Tu, G. Zhao, Y. Zhen, H. Geng, Y. Yi, Z. Wang, H. Zhang, C. Xu, J. Liu, X. Lu, X. Fu, Q. Zhao, X. Zhang, D. Ji, L. Jiang, H. Dong and W. Hu, *Adv. Mater.*, 2014, DOI: 10.1002/adma.201404806.
10 B. Sun, W. Hong, Z. Yan, H. Aziz and Y. Li, *Adv. Mater.*, 2014, **26**, 2636.
11 Y. Zhao, Y. Guo and Y. Liu, *Adv. Mater.*, 2013, **25**, 5372.
12 J. E. Anthony, A. Facchetti, M. Heeney, S. R. Marder and X. Zhan, *Adv. Mater.*, 2010, **22**, 3876.
13 H. Dong, C. Wang and W. Hu, *Chem. Commun*. 2010, **46**, 5211.
14 D. Shukla, S. F. Nelson, D. C. Freeman, M. Rajeswaran, W. G. Ahearn, D. M. Meyer and J. T. Carey, *Chem. Mater.* 2008, **20**, 7486.
15 H. E. Katz, A. J. Lovinger, J. Johnson, C. Kloc, T. Siegrist, W. Li, Y.-Y. Lin and A. Dodabalapur, *Nature*, 2000, **404**, 478.
16 Z. Liu, G. Zhang, Z. Cai, X. Chen, H. Luo, Y. Li, J. Wang and D. Zhang, *Adv. Mater.*, 2014, **26**, 6965.
17 F. Wuerthner and M. Stolte, *Chem. Commun.*, 2011, **47**, 5109.
18 X. Gao, C.-a. Di, Y. Hu, X. Yang, H. Fan, F. Zhang, Y. Liu, H. Li and D. Zhu, *J. Am. Chem. Soc.*, 2010, **132**, 3697.
19 R. Steyrleuthner, R. Di Pietro, B. A. Collins, F. Polzer, S. Himmelberger, M. Schubert, Z. Chen, S. Zhang, A. Salleo, H. Ade, A. Facchetti and D. Neher, *J. Am. Chem. Soc.*, 2014, **136**, 4245.
20 H. Tian, Y. Han, C. Bao, D. Yan, Y. Geng and F. Wang, *Chem. Commun.*, 2012, **48**, 3557.
21 S. Dong, H. Zhang, L. Yang, M. Bai, Y. Yao, H. Chen, L. Gan, T. Yang, H. Jiang, S. Hou, L. Wan and X. Guo, *Adv. Mater.*, 2012, **24**, 5576.
22 H. Minemawari, J. Tsutsumi, S. Inoue, T. Yamada, R. Kuma and T. Hasegawa, *Appl. Phys. Express*, 2014, **7**, 091601.
23 M. L. Tang, M. E. Roberts, J. J. Locklin, M. M. Ling, H. Meng and Z. Bao, *Chem. Mater.*, 2006, **18**, 6250.
24 J. Arient, *RUSS CHEM REV.*, 1965, **34**, 826.
25 P. Deng, Y. Yan, S.-D. Wang and Q. Zhang, *Chem. Commun.*, 2012, **48**, 2591.
26 J. Zhao, J. I. Wong, C. Wang, J. Gao, V. Z. Y. Ng, H. Y. Yang, S. C. J. Loo and Q. Zhang, *Chem. Asian J.*, 2013, **8**, 665.
27 J. Zhao, J. I. Wong, J. Gao, G. Li, G. Xing, H. Zhang, T. C. Sum, H. Y. Yang, Y. Zhao, S. L. Ake Kjelleberg, W. Huang, S. C. Joachim Loo and Q. Zhang, *RSC Adv.*, 2014, **4**, 17822.

Physical Chemistry Chemical Physics Accepted Manuscript

28 J. Zhao, G. Li, C. Wang, W. Chen, S. C. J. Loo and Q. Zhang, *RSC Adv.*, 2013, **3**, 9653.
29 R. P. Ortiz, H. Herrera, C. Seoane, J. L. Segura, A. Facchetti and T. J. Marks, *Chem. Eur. J.*, 2012, **18**, 532.
30 R. P. Ortiz, H. Herrera, R. Blanco, H. Huang, A. Facchetti, T. J. Marks, Y. Zheng and J. L. Segura, *J. Am. Chem. Soc.*, 2010, **132**, 8440.
31 R. P. Ortiz, H. Herrera, M. J. Mancheno, C. Seoane, J. L. Segura, P. M. Burrezo, J. Casado, J. T. L. Navarrete, A. Facchetti and T. J. Marks, *Chem. Eur. J.*, 2013, **19**, 12458.
32 J. Shao, J. Chang and C. Chi, *Chem. Asian. J.*, 2014, **9**, 253.
33 C. Tozlu, S. Erten-Ela and S. Icli, *Sensors and Actuators A: Physical*, 2010, **161**, 46.
34 D. Hanifi, D. Cao, L. M. Klivansky and Y. Liu, *Chem. Commun.*, 2011, **47**, 3454.
35 X. Li, Y. Xiao and X. Qian, *Org. Lett.*, 2008, **10**, 2885.
36 Y. Zhang, D. Hanifi, S. Alvarez, F. Antonio, A. Pun, L. M. Klivansky, A. Hexemer, B. Ma and Y. Liu, *Org. Lett.*, 2011, **13**, 6528.
37 A. Babel and S. A. Jenekhe, *J. Am. Chem. Soc.*, 2003, **125**, 13656.
38 H. Usta, A. Facchetti and T. J. Marks, *Acc. Chem. Res.*, 2011, **44**, 501.
39 S. Ando, J. I. Nishida, H. Tada, Y. Inoue, S. Tokito and Y. Yamashita, *J. Am. Chem. Soc.*, 2005, **127**, 5336.
40 M. L. Tang, J. H. Oh, A. D. Reichardt and Z. Bao, *J. Am. Chem. Soc.*, 2009, **131**, 3733.
41 Q. Meng and W. Hu, *Phys. Chem. Chem. Phys.*, 2012, **14**, 14152.
42 M. L. Tang, A. D. Reichardt, P. Wei and Z. Bao, *J. Am. Chem. Soc.*, 2009, **131**, 5264.
43 A. Lv, S. R. Puniredd, J. Zhang, Z. Li, H. Zhu, W. Jiang, H. Dong, Y. He, L. Jiang, Y. Li, W. Pisula, Q. Meng, W. Hu and Z. Wang, *Adv. Mater.*, 2012, **24**, 2626.
44 N. M. Shavaleev, H. Adams, J. Best and J. A. Weinstein, *J. Organomet. Chem.*, 2007, **692**, 921.
45 J. Locklin, M. E. Roberts, S. C. B. Mannsfeld and Z. Bao, *J Macromol Sci Polymer Rev*, 2006, **46**, 79.
46 M. H. Yoon, C. Kim, A. Facchetti and T. J. Marks, *J. Am. Chem. Soc.*, 2006, **128**, 12851.
47 L.-L. Chua, J. Zaumseil, J.-F. Chang, E. C. W. Ou, P. K. H. Ho, H. Sirringhaus and R. H. Friend, *Nature*, 2005, **434**, 194.
48 A. A. Virkar, S. Mannsfeld, Z. A. Bao and N. Stingelin, *Adv. Mater.*, 2010, **22**, 3857.
49 H. L. Dong, L. Jiang and W. P. Hu, *Phys. Chem. Chem. Phys.*, 2012, **14**, 14165.
50 Y. Ito, A. A. Virkar, S. Mannsfeld, J. H. Oh, M. Toney, J. Locklin and Z. Bao, *J. Am. Chem. Soc.*, 2009, **131**, 9396.
51 A. Y. Amin, A. Khassanov, K. Reuter, T. Meyer-Friedrichsen and M. Halik, *J. Am. Chem. Soc.*, 2012, **134**, 16548.
52 C. Kloc, P. G. Simpkins, T. Siegrist and R. A. Laudise, *J. Cryst. Growth*, 1997, **182**, 416.
53 R. Li, W. Hu, Y. Liu and D. Zhu, *Acc. Chem. Res.*, 2010, **43**, 529.
54 G. Zhao, H. Dong, H. Zhao, L. Jiang, X. Zhang, J. Tan, Q. Meng and W. Hu, *J. Mater. Chem.*, 2012, **22**, 4409.
55 L. Jiang, J. Gao, E. Wang, H. Li, Z. Wang, W. Hu and L. Jiang, *Adv. Mater.*, 2008, **20**, 2735.

Physical Chemistry Chemical Physics Accepted Manuscript

 This journal is © The Royal Society of Chemistry 2012

Journal Name RSCPublishing

COMMUNICATION

Table of Contents:

An Asymmetric Naphthalimide Derivative for n-Channel Organic Field-Effect Transistors

Zongrui Wang, Jianfeng Zhao, Huanli Dong, Ge Qiu, Qichun Zhang, and Wenping Hu

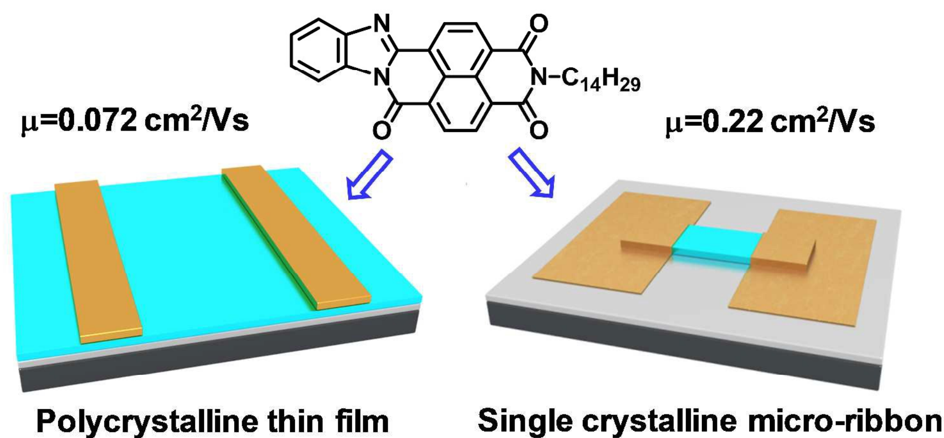

A novel asymmetric naphthalimide derivative (IZ0) is synthesized and high electron mobility of 0.072 $cm^2 V^{-1} s^{-1}$ and 0.22 $cm^2 V^{-1} s^{-1}$ are achieved for IZ0 film and single crystal-based transistors, respectively.

Physical Chemistry Chemical Physics Accepted Manuscript